Model lipid bilayers mimic non-specific interactions of gold nanoparticles with macrophage plasma membranes

Model lipid bilayers mimic non-specific interactions of gold nanoparticles with macrophage plasma membranes

Costanza Montis[a*], Viola Generini[a], Giulia Boccalini[b], Paolo Bergese[c], Daniele Bani[b], Debora Berti[a]

[a]Department of Chemistry and CSGI, University of Florence, Via della Lastruccia 3, 50019 Sesto Fiorentino, Florence, Italy.

[b]Department of Experimental and Clinical Medicine, University of Florence, Viale Pieraccini 6, 50139 Florence, Italy.

[c]Department of Molecular and Translational Medicine, CSGI and INSTM, University of Brescia, 25123 Brescia, Brescia, Italy.

* **Corresponding author:** Costanza Montis E-mail: montis@csgi.unifi.it Tel +390554573017

ABSTRACT: Understanding the interaction between nanomaterials and biological interfaces is a key unmet goal that still hampers clinical translation of nanomedicine. Here we investigate and compare non-specific interaction of gold nanoparticles (AuNPs) with synthetic lipid and wild type macrophage membranes. A comprehensive data set was generated by systematically varying the structural and physicochemical properties of the AuNPs (size, shape, charge, surface functionalization) and of the synthetic membranes (composition, fluidity, bending properties and surface charge), which allowed to unveil the matching conditions for the interaction of the AuNPs with macrophage plasma membranes *in vitro*. This effort directly proved for the first time that synthetic bilayers can be set to mimic and predict with high fidelity key aspects of nanoparticle interaction with macrophage eukaryotic plasma membranes. It then allowed to model the experimental observations according to classical interface thermodynamics and in turn determine the paramount role played by non-specific contributions, primarily electrostatic, Van der Waals and bending energy, in driving nanoparticle-plasma membrane interactions.

KEYWORDS: gold nanoparticles; gold nanorods; biomimetic membranes; supported lipid bilayers; giant unilamellar vesicles; nanomedicine

1. Introduction

Despite the abundance of fundamental and applied studies related to the *in vitro* therapeutic effects of inorganic nanoparticles (NPs), understanding the interaction of synthetic nanostructured matter with biological interfaces, and in particular cell membranes, is still an open challenge towards an effective clinical translation of nanotechnology and nanotoxicology related issues [1–7]. NPs injected in biological fluids are rapidly coated by a shell of biomolecules (often referred as corona) that, in subtle combination with the size and shape of the particles, (re)define the NP biological identity, including their interaction with cells and internalization pathways [8,9]. The first step of NP entry into cells is determined by their interaction with the cell membrane, which can lead to four main endocytosis mechanisms for mammalian cells, including phagocytosis, pinocytosis, caveolae endocytosis and clathrin mediated endocytosis [4,10]. This first step is often "non-specifically" driven by the high binding affinity of the NPs for the lipid membrane, which originates from the NPs excess surface energy. The biomembrane activity of inorganic or polymeric NPs, *i.e.* their tendency to structurally modify and/or permeate natural membranes, has been addressed in several studies on model synthetic membrane structures, as Giant Unilamellar Vesicles (GUVs) and Supported Lipid Bilayers (SLB) [11–13]. These reports suggest that several effects on membrane morphology, permeability and fluidity, such as formation of NP clusters onto the lipid bilayer or formation of lipid-raft-like domains, are driven by this first contact, and that they can be conveniently treated as a multiscale phenomenon to better capture the effect of the protein corona [14]. However, to date, a rational correlation between the findings on synthetic and real cell membranes is still lacking. We report here a first attempt in this direction. A library of gold nanoparticles (AuNPs), systematically covering sizes, charge, shape and coatings, with respect to nanomedicine

applications, was prepared and tested in parallel on zwitterionic and anionic synthetic bilayers and eukaryotic immune system macrophage cells. The membrane activity of these NPs was investigated for free-standing (GUVs) and solid supported (SLBs) lipid bilayers of the same composition, with the twofold purpose to highlight the effect of membrane fluidity and to compare the insights from surface-based and solution techniques. Both GUVs and SLBs can be described as planar membranes [15], but the presence of a solid support in the latter case dramatically increases the energy necessary to bend the bilayer with respect to a GUV with the same composition. Macrophage cells were selected as they are involved in the immune system responses and reaction to external agents, and therefore they are highly relevant in the study of exogenous NP phagocytosis and toxicity [16]. NP-membrane interactions were monitored with Transmission Electron Microscopy (TEM) and Confocal Laser Scanning Microscopy (CLSM) and interpreted within the framework of the DLVO theory, which allowed us to provide a proof-of concept of the fidelity of solid-supported and free-standing synthetic bilayers as mimics of cell plasma membranes, with respect to unspecific interactions with inorganic NPs.

2. MATERIALS AND METHODS

2.1 Chemicals: Gold(III) chloride trihydrate (≥99.9%), Sodium citrate dihydrate (≥99.9%), poly(ethylene glycol) methyl ether thiol, (11-Mercaptoundecyl)-N,N,N-trimethylammonium bromide ((≥90%), 11-mercaptoundecanoic acid (98%), Hexadecyltrimethylammonium bromide ((≥99%), octanethiol (≥98.5%), ascorbic acid (≥98%), $AgNO_3$ (≥99%), toluene (99.8%), MeOH (99.8%), EtOH (≥99.8%), $CHCl_3$ (≥99%), CH_2Cl_2 (≥99.8%), THF (≥99.9%), boric acid (≥99.5%), NaCl (≥99.5%), Calcium chloride hydrate (99.999%), Tetraoctylammonium bromide (98%), glucose (≥99.5%), sucrose (≥99.5%), borax (≥99%), $NaBH_4$ (≥98%) were provided by Sigma-Aldrich (St. Louis, MO). The same for Fetal Bovine Serum (FBS) and (3-(4,5-

dimethylthiazol-2-yl)-2,5-diphenyltetrazolium bromide (MTT) for cells treatment. CellMask™ Orange Plasma membrane stain and β-Bodipy 2-(4,4-diuoro-5,7-dimethyl-4-bora-3a,4adiaza-sindacene- 3-pentanoyl)-1 hexadecanoyl-sn-glycero-3-phosphocholine were purchased from Invitrogen Life Technologies (Heidelberg, Germany), while $DiIC_{20}$ (1,1'-dieicosanyl-3,3,3',3'-tetramethylindocarbocyanine perchlorate) was purchased from Molecular Targeting Technologies (Westchester, PA). 1-palmitoyl-2-oleoyl-sn-glycero-3-phosphocholine (POPC, >99%) and 1-palmitoyl-2-oleoyl-*sn*-glycero-3-phospho-(1'-*rac*-glycerol) (sodium salt) (POPG, >99%) are from Avanti Lipids (Alabaster, AL). All chemicals were used as received. Milli-Q grade water was used in all preparations.

2.2. GUVs preparation: Giant Unilamellar Vesicles were prepared through electroformation. [17–19] Briefly, a POPC or POPG:POPC 1:1 0.5 mg/ml stock solution in $CHCl_3$ was prepared and 0.1% with respect to the total lipid amount of the fluorescent dye (β-Bodipy) was added. 10 μl of the stock solution were deposited on each of two ITO-coated glass slides, on the conductive side. Chloroform was dried under vacuum for two hours and a dry lipid film on each sheet was obtained. The electroformation chamber was prepared sandwiching the sheets with an O-ring separating the lipid films. The chamber was filled with an aqueous solution of sucrose 15 mM, and the electrical contact between the sheets was provided by putting on each sheet a copper tape connected to a pulse generator, set at a sinusoidal alternating voltage of 10 Hz frequency and 2 Vpp amplitude for two hours. GUVs were employed within 24 hours after preparation.

2.3. SLBs Preparation For Small Unilamellar Vesicles preparation the proper amount of POPC or POPG and POPC was dissolved in chloroform/methanol 6:1 (v/v). A lipid film was obtained by evaporating the solvent under a stream of nitrogen and overnight vacuum drying. The film was then swollen and suspended in warm (50°C) NaCl 100 mM solution by vigorous vortex

mixing. To prepare Unilamellar vesicles (ULV) with narrow distribution, the dispersion was then tip-sonicated for 30 minutes. SLB were prepared by adding 10 mM $CaCl_2$ to the vesicles' dispersion and subsequently injecting the vesicles in a chamber containing a coverglass on the bottom. A stable SLB layered on the coverglass was obtained by rinsing the vesicles' dispersion with pure milliQ water, after incubation of the vesicles with the coverglass for twenty minutes at r.t.. To fluorescently label the SLB, a small amount of fluorescent probes (β-Bodipy and $DiIC_{20}$), *i.e.*, 0.1% mol:mol with respect to total lipid amount was added.

2.4. Cell culture Mouse RAW 264.7 macrophages were obtained from the European Collection of Cell Cultures (ECACC, Salisbury, UK). Cells were maintained in Dulbecco's modified Eagle medium (DMEM) supplemented with 10% fetal bovine serum (Gibco Invitrogen, Milan, Italy), 100 U/ml penicillin-streptomycin, 1% L-glutamine 200 mM, (Sigma-Aldrich, Milan, Italy) and 4.5 g/l glucose, and grown in 5% CO_2 atmosphere at 37 °C.

2.5. Confocal Laser Scanning Microscopy (CLSM): CLSM experiments were carried out with a laser scanning confocal microscope Leica TCS SP2 (Leica Microsystems GmbH, Wetzlar, Germany) equipped with a 63x water immersion objective. The 488 nm laser line was employed to detect β-Bodipy fluorescence (λexcitation 488 nm, λ emission 498 nm - 530 nm); the 561 nm laser line was employed to detect $DiIC_{20}$ and Cell Mask dye inside the cells' membrane (λexcitation 561 nm, λ emission 571 nm - 650 nm); the 633 nm laser line was employed to detect AuNP scattering (λexcitation 633 nm, λ emission 620 nm - 640 nm). For experiments on AuNPs interaction with GUVs, 60 µl of GUV dispersion in Sucrose 15 mM were put in a chamber (Lab-Tek Chambered 1.0 Borosilicate Coverglass System, Nalge Nunc International, Rochester, NY USA) and then diluted adding 140 µl of Glucose 15 mM. 100 µl of 5 nM gold nanoparticles' solution was added to GUV dispersions in the chambers. Samples containing nanoparticles and

GUVs were incubated for two hours before the acquisition of the images. For experiments on AuNPs interaction with SLBs, SLB were prepared on a microscope borosilicate coverglass which was put in a home- built measurement chamber. 100 µl of 5nM gold nanoparticles' solution was added in the chambers and the system was incubated for two hours. For experiments on AuNPs interaction with macrophages, RAW 264.7 cells ($5x10^4$/well) were grown on glass coverslips and subjected to the different treatments. After incubation with the nanoparticles, the cells were stained using CellMask Plasma Membrane Stains (Invitrogen, Milan, Italy), as reported in the manufacturer's instructions.

2.6. Transmission electron microscopy on cells After treatments, RAW 264.7 cells were pelleted by centrifugation, fixed in 4% glutaraldehyde and 1% osmium tetroxide and embedded in Epon 812. Ultrathin sections were stained with uranyl acetate and alkaline bismuth subnitrate and examined under a JEM 1010 electron microscope (Jeol,Tokyo, Japan) at 80 KV.

2.7. MTT viability assay Cell viability was measured using the 3-(4,5-dimethylthiazol-2-yl)-2,5-diphenyl tetrazolium bromide (MTT) assay (Sigma-Aldrich). RAW 264.7 cells (10^5/well) were seeded in 96-well plates. At end of treatments, MTT stock solution was added to each well and incubated for 4 h at 37°C. Dimethyl sulfoxide was added to each well to dissolve the formazan crystals. The plate was gently shaken for 10 min. and it was read at 550 nm on a plate reader. Optical density was assumed as indicator of mitochondrial activity and, indirectly, cell viability. The reported data are expressed as the mean ± SEM of at least 3 independent experiments. As the experimental values in each group approximated to a normal distribution, statistical comparison of differences between groups was carried out using one-way ANOVA followed by Student-Newman-Keuls multiple comparison test. A p value ≤ 0.05 was considered

significant. Calculations were done using GraphPad Prism 2.0 statistical program (GraphPad Software, San Diego, CA, USA).

3. RESULTS

3.1 Characterization of AuNPs and membranes

Figures 1 a-c show representative Transmission and Scanning Electron Microscopy (TEM, SEM) images of the synthesized AuNPs, while Dynamic Light Scattering (DLS) and Zeta Potential data are reported in the table (Figure 1d). A full description both of the synthetic procedure and of the characterization (TEM, DLS, Small-Angle X-ray Scattering (SAXS), UV-Vis absorbance and Zeta Potential) are reported in the SI. The Turkevich-Frens method [20,21] leads to citrate-capped gold nanospheres (AuNS@CT, anionic) with core diameter below 15 nm (TEM, Figure 1a), mean hydrodynamic diameter around 20 nm and highly negative zeta potential (around -70 mV, Figure 1d).

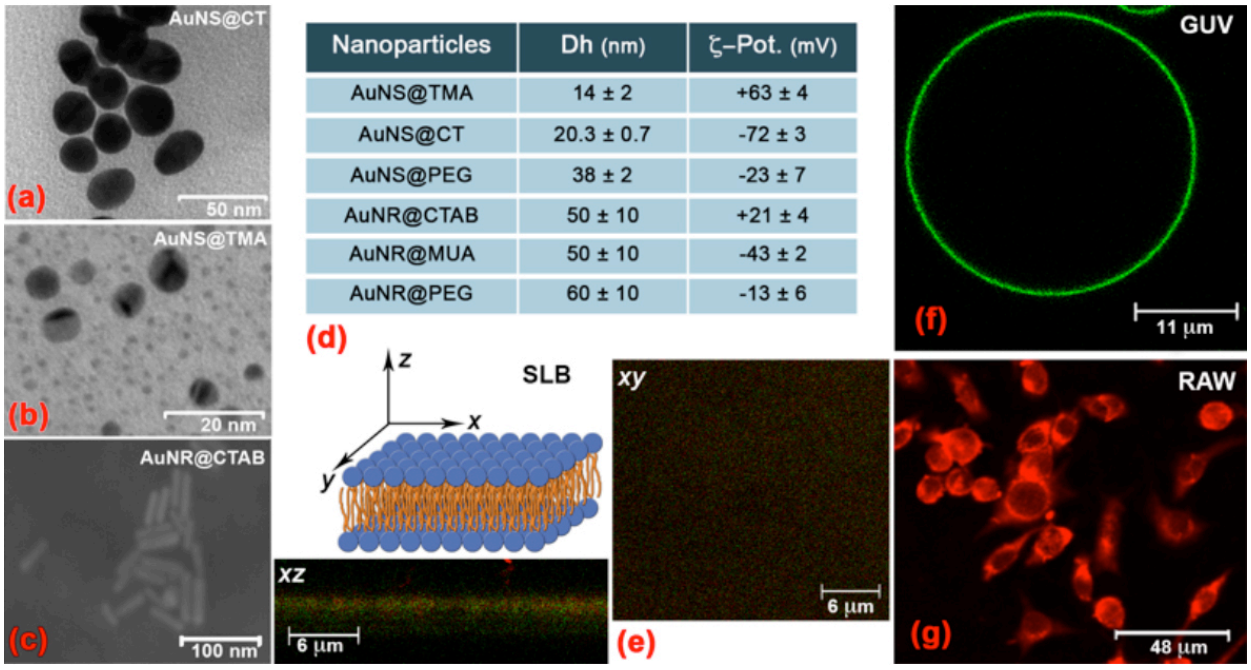

Nanoparticles	Dh (nm)	ζ–Pot. (mV)
AuNS@TMA	14 ± 2	+63 ± 4
AuNS@CT	20.3 ± 0.7	-72 ± 3
AuNS@PEG	38 ± 2	-23 ± 7
AuNR@CTAB	50 ± 10	+21 ± 4
AuNR@MUA	50 ± 10	-43 ± 2
AuNR@PEG	60 ± 10	-13 ± 6

Figure 1. Physichemical characterization of the systems under investigation. (a-c) Representative TEM (a, b) and SEM (c) images of as-synthesized gold nanoparticles: (a) citrate-coated gold nanospheres (AuNS@CT), (b) TMA-coated gold nanospheres (AuNS@TMA), (c) CTAB-coated gold nanorods (AuNR@CTAB); (d) Table summarizing the sizes (Dh) and ζ-Potential of the different AuNPs, synthesized as described in the experimental section; (e, f) Representative LSCM images of the lipid membrane models: (e) horizontal (xy) and vertical (xz) sections of as-prepared POPC SLB, fluorescently labelled with 0.1% w/w β-Bodipy and DiIC20, (f) POPC GUV fluorescently labelled with 0.1% w/w β-Bodipy; (g) Representative LSCM image of RAW cells with the cell membrane fluorescently-labelled, as described in the experimental section.

These nanoparticles were then capped with polyethylene glycol (PEG), through ligand-exchange [22], which increases the mean hydrodynamic diameter to 38 nm, and decreases the absolute value of the zeta potential to -23 mV, due to the extensive uncharged PEG cushion. Cationic nanospheres (AuNS@TMA) were synthesized according to a two-step route [23,24], yielding smaller and better polydisperse spheres with mean hydrodynamic diameter of 14 nm, metal core diameter of 2-3 nm, and positive zeta potential (+63 mV). The same surface functionalizations were performed on gold nanorods, of approximately 10 nm width and 40 nm length (4 as aspect ratio, see SEM image, Figure 1c) and with, respectively, highly negative (AuNR@MUA), slightly negative (AuNR@PEG) and positive (AuNR@CTAB) zeta potentials. Figure 1e and 1f show the confocal laser scanning microscopy (CLSM) images of the membrane models challenged with AuNPs. GUVs prepared through electroformation [17,25], are unilamellar spherical vesicles of polydisperse diameters, from some to some tens of microns, doped with the fluorescent lipid tag β-Bodipy (0.1% mol:mol, green, Figure 1f). Figure 1g displays macrophage RAW cells containing a fluorescent probe in the cell membrane (red), labeled as described in the experimental section. In the absence of NPs the cells shape varies from globular to elongated, with a well defined internal nucleus (which is unlabeled) and with the fluorescent probe evenly distributed along the whole cell membrane.

3.2 Interaction of Au nanospheres with target membranes

Figure 2a shows representative confocal microscopy images of zwitterionic POPC GUVs challenged with 4 nM anionic AuNS@CT after two hours incubation. Even if the GUVs appear intact, *i.e.,* no membrane disruption is evidenced, their size is generally decreased, if compared to the control sample (see Figure 1f), the section is not perfectly circular and some clustering is present. This vesicle clustering is nucleated by NP aggregates, highlighted as orange (AuNP scattering, 633 nm) or black (transmission), spots localized in the adhesion regions between lipid membranes. These interactions are not observed for POPG:POPC GUVs, *i.e.,* when the negative charge of the bilayer is increased (images not reported). Figure 2b shows POPC SLBs after interaction with the same anionic NPs. No morphology perturbations are observed and the probe green fluorescence is homogeneous. However, when Au is imaged with transmission and scattering (Figure 2b), the formation of NPs clusters on SLB surface is clear; even if the solid support rigidifies the inner membrane side, the lipids the upper leaflet can still interact with NPs, which adhere and cluster on it. The NPs adhesion is not evenly distributed on the bilayer, but rather forms aggregates with sizes of some tens μm, not observed on POPG:POPC SLB. This clustering evidences that upon interaction with the lipid membrane, the electrostatic repulsion between like-charged NPs is screened, promoting aggregation.

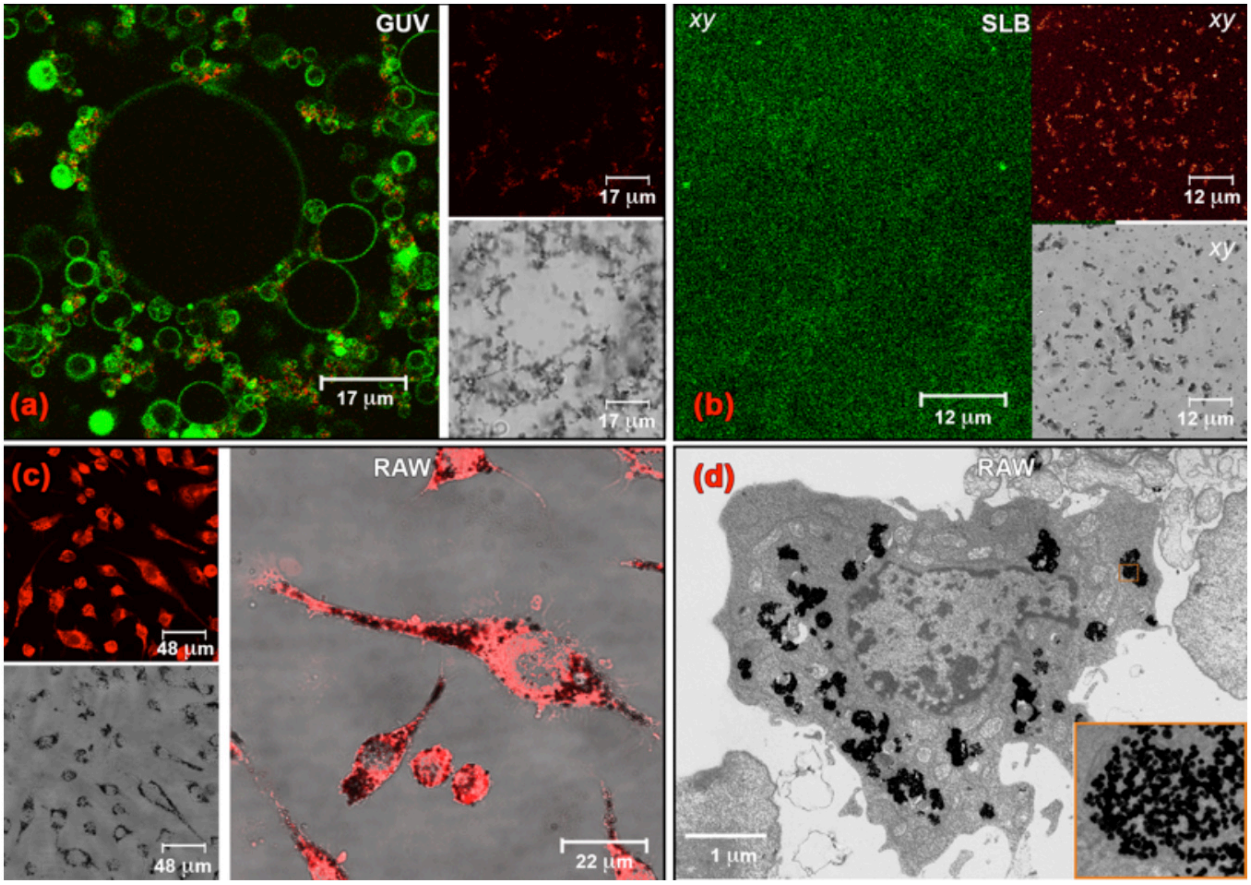

Figure 2. Anionic AuNS@CT and membrane models (panels a, b) and macrophage cells (panels c, d). (panel a) CLSM of AuNS@CT incubated with POPC GUVs, after two hours: (left) overlay of β-Bodipy fluorescence emission (lipid membrane, green) and AuNPs scattering (orange); (right) separated AuNPs scattering (orange) and transmission (greyscale) images acquired in the same field. (panel b) CLSM of the AuNPs incubated with POPC SLB, after two hours incubation (horizontal section). β-Bodipy fluorescence emission (green), AuNPs scattering (orange), transmission (greyscale). (panel c) CLSM of macrophage cells incubated with AuNPs. Cell membrane label fluorescence (red), transmission (greyscale). (panel d) TEM image acquired for AuNPs incubated with macrophage cells.

When the same nanoparticles are incubated with macrophages (Figure 2c), the effects are very similar: relatively small NP clusters are formed solely on the surface of the cells, *i.e.*, not in the surrounding medium, confirming the hypothesis that also for real cells it is the lipid membrane that induces clusterization. No permanent membrane disruption or significant morphological

variations are detected upon exposure to NPs (Figure 1g), similarly to what observed for GUVs and SLBs. TEM images of the cells show NPs in the cytoplasm, which appear internalized as small clusters through the normal uptake routes. We can hypothesize that NPs cluster on the cell surface thanks to the membrane templating effect and are then internalized in the cell [26,27]. After internalization the cytoplasm is unmodified with respect to the control experiment (see SI for comparison).

Concerning AuNS@PEG, their interaction with POPC GUVs does not produce apparent variations: the GUVs remain perfectly spherical (green fluorescence of β-Bodipy), and the nanoparticles only occasionally form clusters (orange spots of Au scattering). This weaker interaction is confirmed for POPC SLBs (Figure 3b): similarly to what observed for AuNS@CT, the lipid membrane appears intact (green β-Bodipy fluorescence is homogeneous and evenly distributed). However, differently from AuNS@CT, cluster formation occurs to a lesser extent. This difference is consistent with the confocal microscopy observations of the interaction of these NPs with cells (Figure 3c). Only rare NPs' clusters are visible on the cell surface (black spots, transmission), while no differences in the number or shape of the cells is observed with respect to the control. This result is consistent with a passivation of the NPs' surface, similar to what observed for the protein corona shell [14] and is fully in line with the well-known behavior of PEG-coated NPs with biological interfaces: while PEG coating generally improves pharmacokinetic properties of nanodrugs or DDS, cell internalization might be significantly decreased [28].

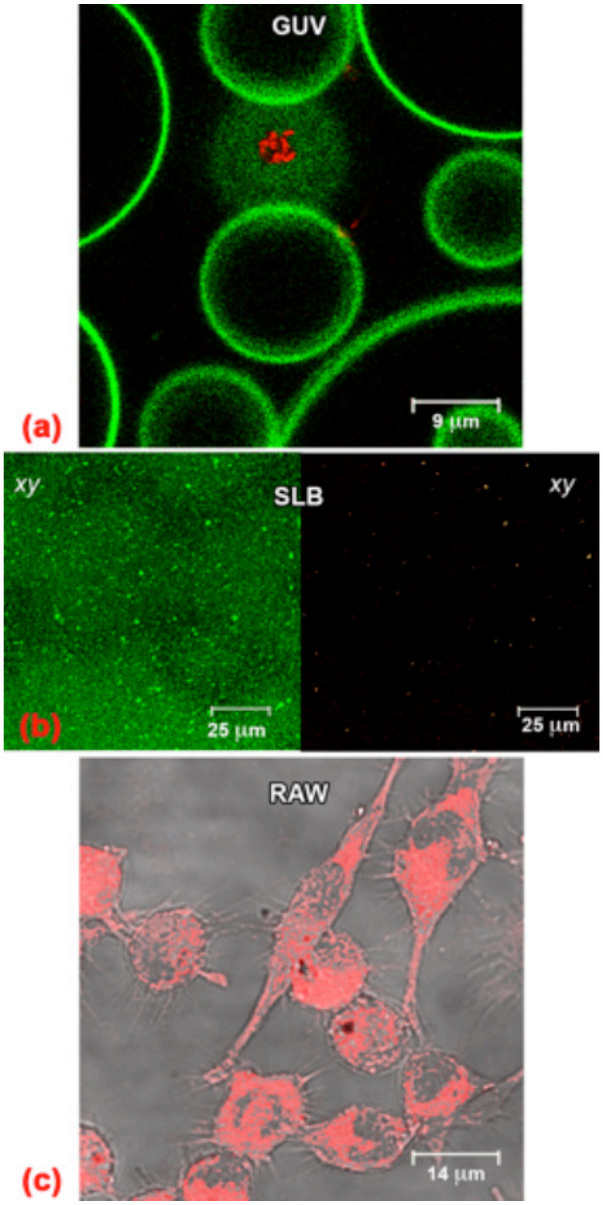

Figure 3. PEG-coated AuNS@PEG with model bilayers (panels a, b) or macrophage cells (panels c). (panel a) CLSM image for AuNS@PEG incubated with POPC GUVs for two hours: overlay of β-Bodipy fluorescence emission (lipid membrane, green) and AuNPs scattering (orange). (panel b) CLSM image for AuNS@PEG incubated with POPC SLB for two hours (horizontal section). β-Bodipy fluorescence emission (green), AuNPs scattering (orange). (panel c) CLSM images of macrophage cells incubated with AuNS@PEG. Overlay of cell membrane label fluorescence (red) and transmission (greyscale).

Finally, when cationic nanospheres (AuNS@TMA) are considered, the interaction with POPC vesicles results in a decrease of the GUVs number density and size. AuNS@TMA disrupt POPC

GUVs resulting in the formation of sub-micron NP-lipid aggregates (see SI in comparison to Figure 1f). This trend is intensified for POPG:POPC GUVs (Figure 4, panel a): NPs penetrate inside GUVs and cluster to form micron-sized aggregates (much larger than the clusters visualized for AuNS@CT interacting with the same GUVs), while the GUVs completely lose their original shape and rupture into star-like structures constituted by hollow tubular assemblies, protruding from a core constituted by the micron-sized NPs' aggregates. For the same lipid composition on a solid support we used a dual fluorescence labeling scheme. When AuNS@TMA NPs are added and tracked thanks to their scattering, large NPs aggregates are formed on the lipid surface of the SLB, coated by both lipid fluorescent probes (see also SI for other representative images): clearly, in this case, the interaction of NPs with the bilayer enables the extraction of lipids even from the lower leaflet of the SLB, in close contact with the support, and the large NPs aggregates are completely wrapped by the lipids forming nanoparticles-lipids complexes; these complexes can be recognized as a first step (in a 2D model) of what observed in the GUVs, where the star-like structures are formed starting from a lipid extraction and the formation of large micron-sized NPs-lipid aggregates. For POPC bilayers, subtler effects emerge (Figure 4 panel b): POPC SLBs are in the fluid phase at room temperature, in the absence of AuNPs, and a homogeneous distribution of the two dyes is highlighted (see Figure 1e). Upon incubation with cationic NPs, a spontaneous lateral phase separation of the fluorescent probes β-Bodipy (green, higher affinity for fluid lipid phases), and $DiIC_{20}$ (red, higher affinity for liquid ordered lipid phases) is observed, with the formation of regions enriched in $DiIC_{20}$ with fractal flowers-like shape. This phase separation indicates the formation of more rigid domains in the areas of adhesion of NPs.

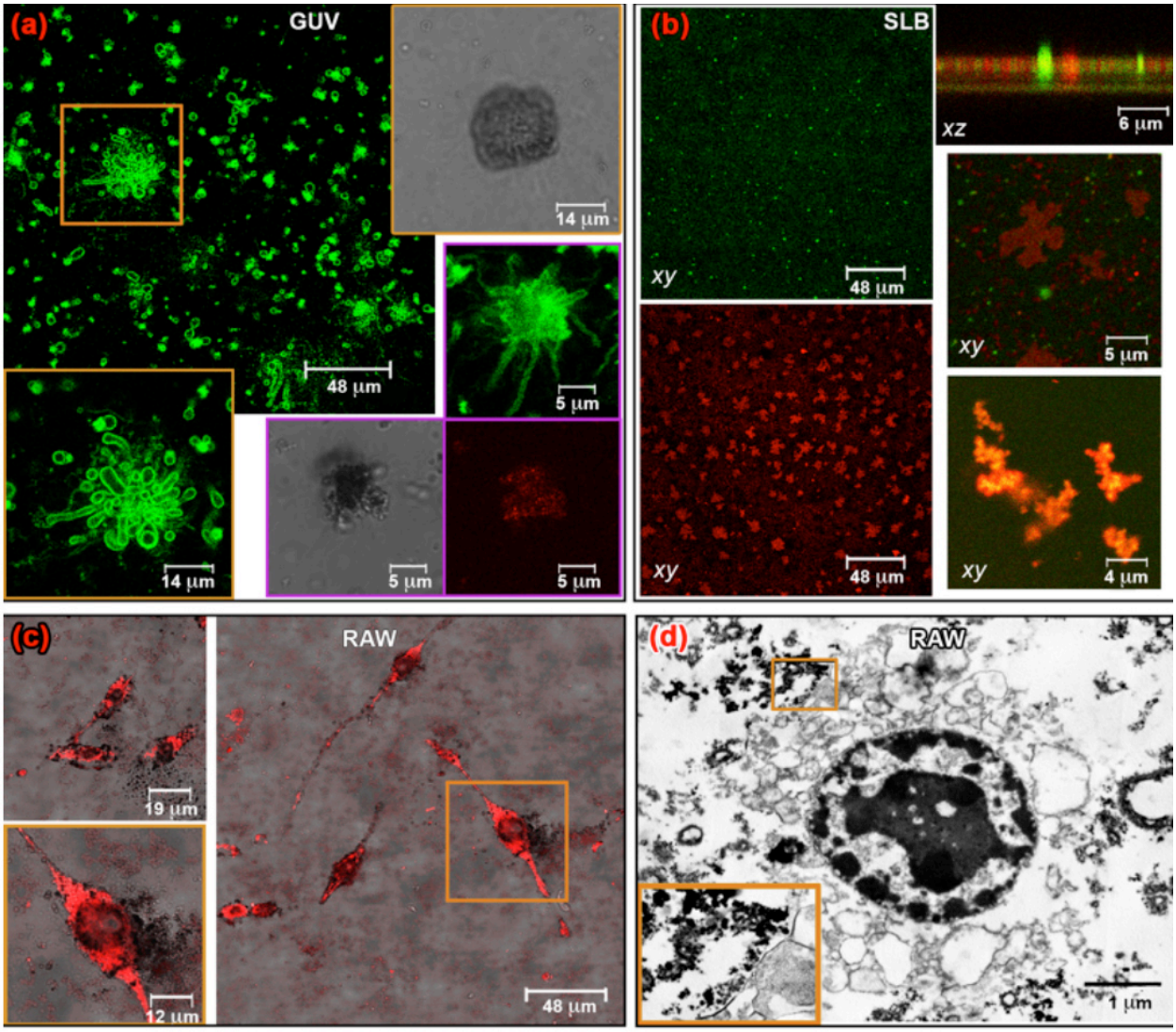

Figure 4. Cationic AuNS@TMA and membrane models (panels a, b) or macrophage cells (panels c, d). (panel a) CLSM image of AuNPs incubated with POPG:POPC 1:1 GUVs, after two hours: β-Bodipy emission (lipid membrane, green), AuNPs scattering (orange), transmission (greyscale) images in the same fields. (panel b) CLSM image of the AuNPs incubated with POPC and POPG:POPC 1:1 SLB, after two hours. (left) horizontal sections (xy) of β-Bodipy (green) and DiIC20 (red) fluorescence emission in the same field of POPC SLBs; (right) vertical (xz) and horizontal (xy) sections of the SLB showing the overlay of β-Bodipy (green) and DiIC20 fluorescence emission (red) of POPC SLBs; representative horizontal (xy) overlay of β-Bodipy (green) and DiIC20 (red) fluorescence emission and AuNPs scattering (orange) of POPG:POPC SLB. (panel c) CLSM images of macrophage cells incubated with AuNPs. Cell membrane label fluorescence (red), transmission (greyscale). (panel d) TEM image acquired for AuNPs incubated with macrophage cells.

Conversely, in the areas not involved in NP adhesion, the membrane remains fluid. This phenomenon has a high biological relevance: bilayer restructuration, together with formation of membrane's rafts and domains, is often connected in real cells to a response to external stimuli In our previous study we detected the formation of small (nm to hundreds of nm size) rigid regions on GUVs membranes upon interaction with anionic AuNPs [14]; here, the formation of micron-size raft-like domains on a model lipid membrane upon interaction with nanoparticles is observed for the first time. Concerning the interaction with macrophage cells (Figures 4c, d), NPs clusterization is observed, similarly to anionic nanoparticles, but in the present case this aggregation is accompanied by partial disruption of cell membrane, whose fluorescently labeled debris can be observed in the surrounding environment (Figure 4c) and by a loss of integrity of the cytoplasmic structure, highlighting a permanent damage.

3.3 Interaction of AuNR with target membranes

Figure 5 collects the results for AuNRs with different coatings incubated with membrane models and macrophage cells. Figure 5a displays representative confocal microscopy images of cationic nanorods (AuNR@CTAB) incubated with POPC GUVs. The main effect is extraction of tubular lipid structures, which grow from the parent sphere, until they breakup into pearls, *i.e.*, a periodic string of smaller ellipsoidal vesicles connected by a narrow neck (see representative movies in the SI). In a previous study we observed the extraction of tubular structures from POPC GUVs, upon interaction with AuNS@CT, but coated with a serum protein corona. These latter structures, smaller than those observed for NRs, were stable and did not break into small vesicles, suggesting a different mechanism. A very similar phenomenon, *i.e.* vesicles' pearling induced by nanoparticles, was observed by Yu [29] for DOPC GUVs and aliphatic amine

nanospheres encapsulated in the vesicles lumen, allowing the NPs to adsorb onto the inner lipid leaflet; the control experiment showed no shape change when the NPs were added from the outside. This may indicate that NRs, differently from NSs, spontaneously penetrate the bilayer, adsorb onto the inner leaflet and cause the protrusion of elongated structures that break through pearling. For PEGylated phospholipid bilayer deformation stops with tubular protrusion ad no pearling is generated.

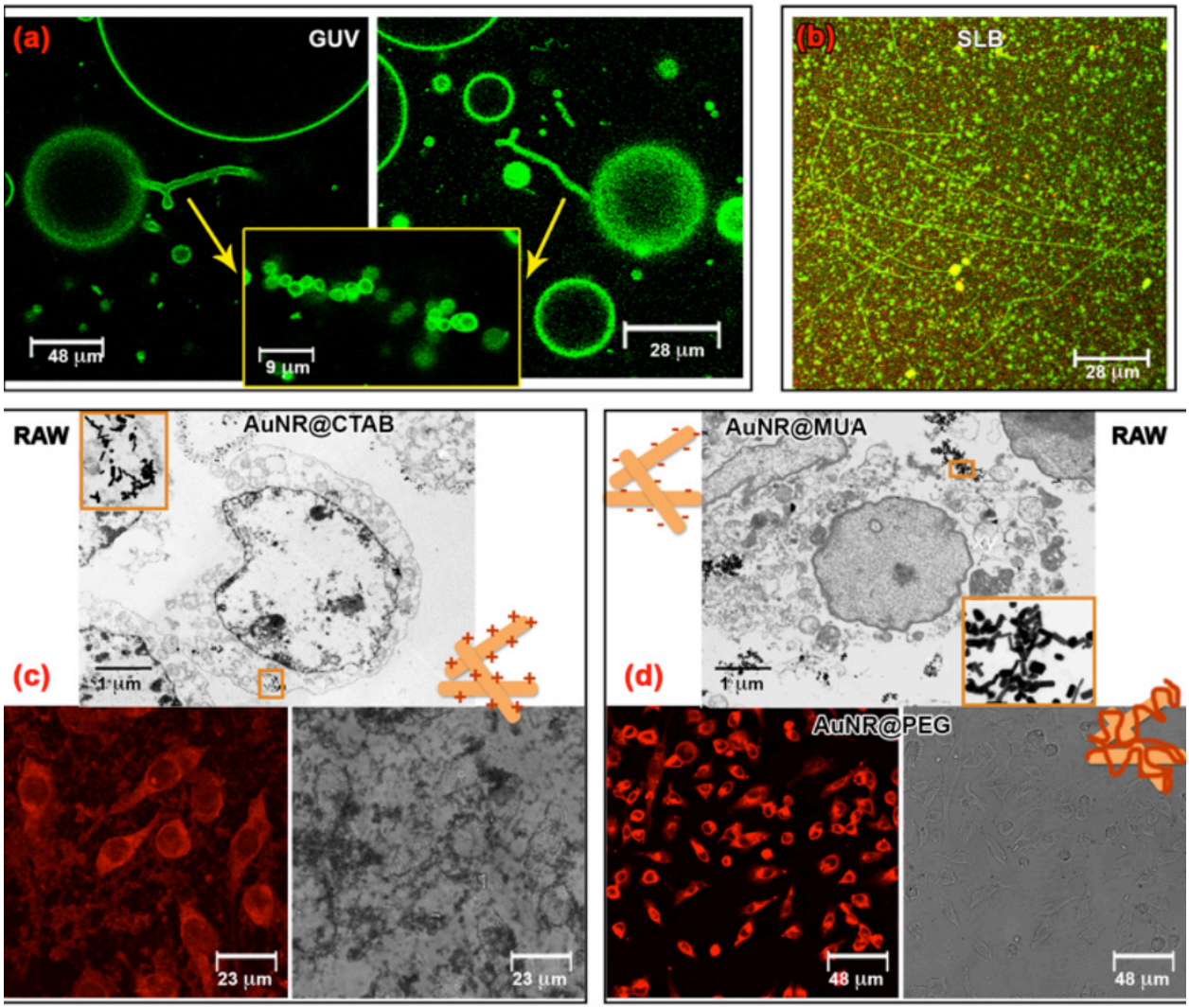

Figure 5. AuNR and membrane models (panels a, b) and macrophage cells (panels c, d). (panel a) CLSM image acquired for the AuNR incubated with GUVs, after two hours incubation: β-Bodipy fluorescence emission (lipid membrane, green). (panel b) CLSM image acquired for the AuNR incubated with SLB, after two hours incubation (horizontal section). Overlay of β-

Bodipy fluorescence emission (green), DiIC20 fluorescence emission (red). (panel c) TEM and CLSM images acquired for macrophage cells incubated with cationic AuNR@CTAB. Cell membrane label fluorescence (red), transmission (greyscale). (panel d) TEM image acquired for macrophage cells incubated with anionic AuNR@MUA and CLSM images acquired for macrophage cells incubated with PEG-coated AuNR@PEG. Cell membrane label fluorescence (red), transmission (greyscale).

Concerning SLBs, AuNRs clearly adhere to them (Figure 5b), forming end-to-end chainlike gold nanorods aggregates coated by lipid molecules. For cationic NRs, AuNR@CTAB interact similarly with POPC and POPG:POPC SLBs membranes; the same pattern is observed for anionic AuNR@MUA/zwitterionic POPC SLBs, while there is no interaction with negative POPC:POPG bilayer. PEGylated nanorods show a weaker interaction with respect to both cationic and anionic nanorods: only small superficial aggregates are observed on POPC SLB instead of the elongated chainlike structures, and no interaction is observed with anionic POPG:POPC 1:1 samples (see SI). When macrophage cells are incubated with cationic nanorods, the cell number substantially decreases, as expected from their well-known toxicity [30], which is clear also from TEM results: upon interaction the cell loses its integrity, while NRs clusters form both on the membrane and inside the cells. Moreover, similarly to what observed for cationic NSs, the confocal microscopy images show the presence of membrane fragments on the chamber bottom, colocalized with AuNRs clusters, which are not visible as isolated entities. We can conclude that lipid extraction from the membrane is clearly provoked by AuNRs, in an identical way as what observed for membrane models. Anionic and PEGylated AuNRs (Figure 5d) have generally milder effect on macrophage cells, but, in striking parallel to what observed for the membrane models, the charged NRs show qualitatively stronger interactions: the TEM images show clusters of AuNRs interacting with cells and clear membrane damage with respect to the control (see SI), while, differently from cationic NRs, the inner cytoplasmic structure is

not disrupted; conversely, our experiments did not evidence any effects for PEG-coated NRs on cells, confirming that the PEG cushion strongly decreases adhesion ability both on lipid membrane models and real cells.

Finally, the same experiments were repeated by passivating with a serum protein corona the NPs with the highest membrane activity, *i.e.*, cationic nanospheres AuNs@TMA and nanorods, AuNR@CTAB (see SI Figure S11). Similarly to what observed for the PEG coating, the interaction is damped: when these nanoparticles are passivated, their membrane-activity (shown in Figures 4 and 5) is completely quenched.

3.4 MTT assays of macrophages incubated with the AuNPs.

In order to formulate a first idea of the biological effects of the different NPs on macrophages metabolism, MTT tests were performed after incubating the NPs with the RAW cells for six hours.

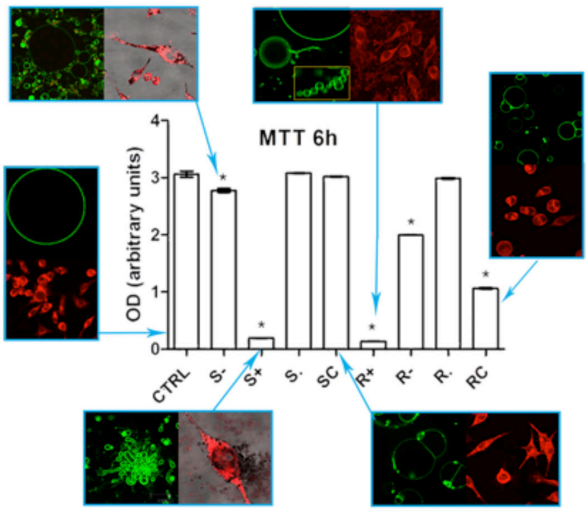

Figure 6. 6 hours MTT assay on macrophages incubated with AuNPs with different shape and functionalization. CTRL control; S- anionic citrated Turkevich nanospheres; S+ cationic nanospheres; S. PEG-coated Turkevich nanoparticles; Sc corona-coated cationic nanospheres; R+ cationic nanorods; R. PEG-coated cationic nanorods; Rc corona-coated cationic nanorods. MTT legend: Significance of differences: *p<0.001 vs. control

Figure 6 shows that, in line with the literature, the main physicochemical features of NPs implied in *in-vitro* toxicity are the surface charge (*i.e.*, cationic NPs are more toxic than anionic ones), the shape anisotropy (*i.e.*, the rods are more toxic than the spheres), the chemical nature of the passivating agent and, possibly, its desorption equilibrium from the particle [30], the surface energy. Both anionic nanospheres and nanorods exhibit a low but significant toxicity with respect to the control, but the presence of a PEG cushion or of a protein corona passivating the cationic coating decreases toxicity. The higher toxicity of cationic nanorods passivated by the corona can be attributed to a lower affinity of proteins for the rod edges.

It is thus apparent that the NP membrane activity, similar for model membranes and real cells, has a strong connection to cell viability, as determined by the MTT assay.

4. DISCUSSION

4.1. NPs-lipid membranes interaction energy: theoretical considerations

The previous results show that the NP membrane activity can be predicted observing the interactions with free standing and solid supported lipid bilayers, composed of homogeneous fluid lipid mixtures, without raft-like domains or embedded membrane proteins. This observation supports the hypothesis that a key role in membrane activity is played by unspecific interactions (*i.e.* not mediated by molecular recognition events) between the NPs and lipid components of the eukaryotic cell membrane. Here we briefly review the different energetic contributions to the potential energy, for our model systems, emphasizing the determining ones for each of the membrane mimics above described.

The NPs-bilayer interaction consists of the following steps (i) adhesion to the bilayer, which depends on the interaction energy between AuNPs and the lipid membrane ($E_{NP\text{-}m}$); (ii) complete or partial wrapping of the NPs by the membrane, depending on the physicochemical features of

the lipid membrane, in particular to its undulation energy term (E_m)[31,32]; (iii) possible clusterization of NPs on the lipid membranes, with a templating role of the bilayer [14,33], implying that steric and electrostatic AuNP-AuNP repulsion ($E_{NP\text{-}NP}$), which guarantee colloidal stability in the bulk liquid phase, are released upon interaction with the membrane:

The total energy will be given by (Eq. 1):

$$E_{int} = E_{NP\text{-}NP} + E_{NP\text{-}m} + E_m \quad (1)$$

In a first approximation, the first two terms, whose balance will determine adhesion to the membrane, can be evaluated according to a classical DLVO formalism, including the repulsive electrical-double layer (E^{EL}) and the attractive van der Waals interactions, (E^{LW}) [31,34,35]. For bulky (e.g. PEG) surface functionalizations, a repulsive steric contribution ($E^{ST}_{NP-NP}(d)$), should be considered, which depends on the length and conformation of the coating molecules.

In the absence of lipid bilayers, $E_{NP\text{-}NP}$ in water (or at low ionic strength) features an electrostatic barrier to aggregation and inorganic NPs dispersions are stabilized by electrostatic (E^{EL}_{NP-NP}) or steric (E^{ST}_{NP-NP}) repulsion.

The second term, $E_{NP\text{-}m}$ can be written considering the interaction between spherical NPs with radius R and a flat lipid membrane of thickness h, separated by a distance d. This approximation holds for GUVs, since they are cell-sized vesicles with negligible curvature, and for SLB, that can be considered as an infinite plan. Again, $E_{NP\text{-}m}$ can be modelled as the sum of London-Van der Waals and electrostatic contributions (Eq. 2 and 3):

$$E^{LW}_{NP-m}(d) = -\frac{AR}{6}\left(\frac{1}{d} - \frac{1}{(d+h)}\right) - \frac{A}{6} ln\left(\frac{d}{d+h}\right) \quad (2)$$

$$E^{EL}_{NP-m}(d) = \frac{\varepsilon R(\psi_{NP}{}^2 + \psi_m{}^2)}{4}\left[\frac{2\psi_{NP}\psi_m}{\psi_{NP}{}^2 + \psi_m{}^2} ln\left(\frac{1+e^{-\kappa d}}{1-e^{-\kappa d}}\right) + ln(1 - e^{-\kappa d})\right] \quad (3)$$

with ψ_m and ψ_{NP} the surface potentials of the membrane and the nanoparticles, respectively. The Hamaker constant is always positive for symmetrical interactions (*i.e*. NP-NP, for AuNPs-AuNPs it is around 2.5×10^{-19} J[36]) and generally positive for asymmetrical interactions, so that E_{NP-m}^{LW} is attractive in most cases (for instance for phospholipid bilayer interacting with oxide nanoparticles, it is around 4×10^{-21} J [31]). Concerning the Coulomb term, biological membranes are negatively charged, so the sign of NPs charge dictates the nature of the electrostatic contribution (E_{NP-m}^{EL}), from attractive (for TMA and CTAB-coated NPs) to repulsive (for CT and MUA-coated NPs). Overall these two terms define the adhesion energy of the NP to the membrane. Then, the interplay between this adhesion energy and E_m (see Eq. 1), accounting for fluidity, spontaneous curvature and bending modulus of the bilayer [37,38], drives the spontaneous wrapping of the NPs by the membrane. The penalty cost required to membrane to wrap the particles is related to the elastic energy of the membrane E_{el}. Considering NPs with small characteristic sizes, compared to the characteristic lengthscales of the membrane, E_{el} is dominated by the bending energy E_{be}, and thus E_m can be expressed as (Eq. 4):

$$E_m \approx E_{el} \approx E_{be} = \int (2\kappa M^2 + \bar{\kappa} K) dA \quad (4)$$

over the membrane area *A*, being *M* and *K* the local mean and Gaussian curvatures, *k* the bending rigidity and $\bar{\kappa}$ the of Gaussian curvature modulus [37,39]. It is possible to define a critical wrapping radius R_c of the NP as (Eq. 5) [31,38]:

$$R_C \equiv \sqrt{2\kappa/|W|} \quad (5)$$

with *W* the adhesion energy per unit area. For a given adhesion energy, the more rigid the membrane, the larger the critical wrapping radius. In other terms, for the same NP/membrane

system, the same NP can be wrapped by a free standing bilayer, but not by a SLB of the same composition. In summary, the balance between these energy contributions determine the occurrence and/or the extent of the most commonly encountered interaction phenomena (adhesion, clusterization, wrapping). Further contributions, such as hydration forces, which are relevant in phospholipid membranes particularly in the description of short range phenomena, hydrophobic interactions, which might be relevant in internalization processes, depletion forces, counterion release, which provides a strong entropic contribution to the binding of oppositely charged polyionic colloids, can be considered to capture subtler details, as discussed in some specific publications [31,34,40]. In the next section, we will discuss our experimental results within this simplified framework.

4.2. Energy balance for NPs-lipid membranes interactions

NPs dispersions, in the absence of lipid membranes, are stabilized against aggregation thanks to electrostatic (CT and TMA-coated NS and CTAB and MUA-coated NR) or steric (PEG-coated particles) repulsive terms. Concerning the interaction of NPs and lipid membranes ($E_{NP\text{-}m}$), the electrostatic contribution (E_{NP-m}^{EL}) is repulsive for anionic NPs (CT and MUA-coated NPs and, to a lesser extent, PEG-coated NPs), and attractive for cationic NPs (TMA and CTAB-coated NPs). In addition, the electrostatic contribution depends on the surface charge density of the membrane, which is slightly negative for zwitterionic POPC membranes and negative for POPG:POPC 1:1. In summary, the electrostatic contributions change from highly repulsive, for AuNS@CT (AuNR@MUA)-POPG:POPC 1:1 membranes, to slightly repulsive for the same systems and POPC membranes, to attractive for AuNS@TMA and AuNR@CTAB-POPC membranes, to highly attractive for the same systems interacting with POPG:POPC 1:1. Steric

stabilization of PEG-coated NP (AuNS@PEG and AuNR@PEG) provides an efficient barrier to membrane adhesion, due to entropic losses.

On a shorter length scale with respect to electrostatics, NPs' adhesion to bilayers is promoted by Van der Waals-London forces contribution (E_{NP-m}^{LW}), depending on the Hamaker constant. Finally, the membrane-related term E_m is repulsive, and depends on the propensity of the membrane to topologically deform from its spontaneous curvature upon interaction with the NPs. This term is much higher for SLBs than for GUVs, due to the close interaction of the lower leaflet of the SLB with the support, almost completely hampering its bending. The balance of these contributions is related to defined and estimable physicochemical features (size, surface potential, Hamaker constant, bending modulus, spontaneous curvature and so on) and controls the interaction of NPs and lipid membranes, driving the phenomena presented and described in the previous paragraphs.

If we consider first the effects of NS on model membranes, for AuNS@CT interacting with free-standing POPC bilayers the Van der Waals-London forces contribution (E_{NP-m}^{LW}) is sufficient to overcome the slight electrostatic repulsion (E_{NP-m}^{EL}). After adhesion, a partial or complete membrane wrapping occurs, highlighted by the presence of spots on GUVs' surface, with the fluorescence of the lipid tag (green) colocalized with Au scattering (orange, Figure 2a). NPs wrapping is then connected to two associated phenomena: the clusterization of the NPs on the lipid membrane, attributable to the (E_{NP-m}^{LW}) contribution in overcoming the NP-NP electrostatic repulsion, and the deformation of the membrane, due to the curvature imposed by the NPs, highlighted by the micron-scale deformation of the GUVs circular shape due to the adhering aggregates of NPs (Figure 2a). These two phenomena are clearly connected to each other

through the critical radius R_C, resulting in a synergistic role of NPs adhesion, wrapping and clusterization, since the radius of curvature imposed to the membrane is lowered for NPs clusters, and the membrane bending energy (E_m) is minimized. In a previous study [14], we observed a more dramatic interaction between AuNS@CT and GUVs in PBS, driven by the high surface energy of the nanoparticles, and supported by the electrostatic screening effect due to the background electrolyte; in this case the clusterization of NPs on the GUVs surface determined the formation of a NPs crust completely coating and even disrupting the membrane integrity. In pure water the initial interaction appears the same: small clusters are formed after adhesion, due to the templating effect operated by the lipid membrane itself. However, in pure water the repulsive electrostatic interaction between like-charged nanoparticles and the slightly negatively charged membrane (E_{NP-m}^{EL}) is not screened, resulting in a less dramatic effects, but prompting a similar mechanism. To confirm this hypothesis, when we increase the electrostatic repulsion (E_{NP-m}^{EL}) by changing the lipid composition (POPG:POPC GUVs), no clusterization occurs, because the term E_{NP-m}^{LW} is not sufficient to promote adhesion. Finally, when E_m increases, moving from GUVs to SLBs (Figure 2b), NPs clusterization onto POPC membranes is still observed, but no membrane perturbation is visible (the fluorescence of the lipid probe is evenly distributed on the surface), suggesting that the adhesion of the NPs on the target membrane, mainly driven by the Van der Waals-London forces (E_{NP-m}^{LW}), is not sufficient to drive membrane deformation necessary for wrapping and clusterization. Taken altogether, this set of results can be rationalized as follows: anionic gold nanospheres, characterized by high surface energy, adhere on lipid membranes, similarly to what observed in previous studies. For PEG-coated NSs the steric stabilization term acts as an effective barrier preventing both NP-NP interaction (leading to clusterization) and NP-membrane adhesion. Accordingly, the clusterization of PEG-

coated NPs on the lipid membranes is not observed. Considering cationic NSs, the dispersions are electrostatically stabilized, but the charge contrast with the membrane makes the relatively long-range E_{NP-m}^{EL} attractive. This induces the formation of micron-sized NP-lipid mixed aggregates, where the GUVs lose their original shape and are partially engulfed in these assemblies. If the same bilayer is spread on a solid support the relatively high E_m prevents wrapping. All of the phenomena that have previously discussed for AuNS@CT NPs from adhesion, to wrapping, to membrane deformation and NPs clusterization templated by the membranes, are emphasized for cationic NPs.

If we consider nanorods, their anisotropy implies the coexistence of regions of high curvature, where the concentration of the capping agent is lower, with flat regions, with lower curvature. NRs have a faceted structure, where the end-facets bind the coating molecules less strongly compared to the side-facets: the end-to-end assembly is facilitated, because the lower ligand amount reduces both steric and electrostatic repulsion and locally increases the surface energy [41]. The NP anisotropy determines realtively high E_{NP-NP}^{LW} and E_{NP-m}^{LW} energy terms, involving the NRs edges and resulting in membrane wrapping and NPs clusterization into end-to-end assemblies. Concerning the different coatings of the NRs, both in the interaction with GUVs and SLBs, the shape of the molecules is the main factor, while the different coatings have minor effects that can be summarized as follows: cationic AuNR@CTAB alter extensively POPG:POPC 1:1 GUVs (high E_{NP-m}^{EL} attraction) and less zwitterionic POPC GUVs (lower E_{NP-m}^{EL} attraction) and anionic AuNR@MUA perturb only zwitterionic POPC GUVs but don't interact with negatively charged POPG:POPC 1:1 GUVs, (E_{NP-m}^{EL} repulsion) this clearly due to an electrostatic contribution to the interaction between the nanorods and the GUVs.

For the purposes of this study, only a qualitative evaluation of the energy contributions to NPs-membranes interaction is provided. Interestingly, this qualitative approach is sufficient to explain the phenomena observed upon incubation of the NPs with lipid membranes. On more quantitative grounds, a precise knowledge of the physicochemical parameters of the nanosystems of interest allows in principle a reliable estimate of each energy contribution to the NPs-membranes interaction potential.

5. CONCLUSIONS

In this manuscript we compare the interaction of AuNPs with biomimetic lipid bilayers (in the form of GUVs and SLBs) to the interaction of the same AuNPs with macrophage plasma membranes. By systematically varying the structural and physicochemical properties of the AuNPs – size, shape (spherical and rod like), charge, surface functionalization – and of the biomimetic membranes – composition, fluidity, bending properties and surface charge – we were able

(i) to perform a systematic and comprehensive investigation on the interaction of NPs with lipid membrane models through Transmission Electron Microscopy (TEM) and Confocal Laser Scanning Microscopy (CLSM), identifying the main contributions at play;

(ii) to establish a relationship between the experimental observations on membrane models with those on macrophage membranes: the clear similarities suggest that biomimetic membranes are reliable models to investigate the nano-bio interfaces phenomena in simplified conditions and prove that unspecific interactions are particularly relevant in determining the interaction pathway of nanoparticles. Furthermore, MTT viability assays on macrophages suggests that the membrane activity of NPs is relevant for cytotoxicity.

(iii) to frame the experimental observations on membrane models and real cells according to simple energetic contributions and propose a unifying interaction energy model for NPs and cell membranes, able to explain phenomena as diverse as lipid-templated NPs clusterization, membrane pearling, raft-like domain formations, lipid extraction, star-like mixed NPs-lipid aggregate formation.

The above findings allowed determining a connection between the physicochemical features of the AuNPs, their interaction pathways with membrane models and their effects on macrophage membranes, proving the underlying role played by non-specific interactions. These findings strengthen the utility of biomimetic membranes as reliable yet simple models to investigate and predict interaction of inorganic nanoparticles with cell membranes.

On a wider perspective, this contributes to advance our understanding of biological response to engineered nanomaterials and widens the toolbox for further investigating it, both crucial needs [1,2] for the development of nanomedicine. In a future perspective, the structural and functional complexity of model membranes should be increased, to finely tune the experimental and theoretical descriptions of the interactions between nanoparticles and cell plasma membrane. The same approach has been successfully used to produce cell-material dynamic interfaces and biosensors, where confinement artifacts are limited at the ligand-receptor recognition [42,43]. Indeed, to test the model validity and prediction accuracy to other nanoparticles of technological and/or biological and/or toxicological relevance (such as SiOx or FeOx NP) and other cell lines would be of general interest and importance.

Acknowledgements

All the authors acknowledge E. Fratini and for S. Tilli assistence in SEM and SDS-Page experiments, respectively.

Appendix A. Supplementary material

Supplementary data associated with this article can be found, in the online version: supplementary materials and methods, additional physicochemical data on the synthesized nanoparticles, supplementary LSCM and TEM images of membrane models and cells before and after interaction with AuNPs, LSCM time-lapse of GUVs interacting with AuNRs.

REFERENCES

[1] W.C.W. Chan, Nanomedicine 2.0, Acc. Chem. Res. 50 (2017) 627–632. doi:10.1021/acs.accounts.6b00629.

[2] C.J. Murphy, A.M. Vartanian, F.M. Geiger, R.J. Hamers, J. Pedersen, Q. Cui, et al., Biological responses to engineered nanomaterials: Needs for the next decade, ACS Cent. Sci. 1 (2015) 117–123. doi:10.1021/acscentsci.5b00182.

[3] E. Rascol, J.-M. Devoisselle, joel c. Chopineau, The relevance of membrane models to understand nanoparticles-cell membrane interactions, Nanoscale. 8 (2016) 4780–4798. doi:10.1039/C5NR07954C.

[4] C.M. Beddoes, C.P. Case, W.H. Briscoe, Understanding nanoparticle cellular entry: A physicochemical perspective, Adv. Colloid Interface Sci. 218C (2015) 48–68. doi:10.1016/j.cis.2015.01.007.

[5] A. Marín-Menéndez, C. Montis, T. Díaz-Calvo, D. Carta, K. Hatzixanthis, C.J. Morris, et al., Antimicrobial Nanoplexes meet Model Bacterial Membranes: the key role of Cardiolipin, Sci. Rep. 7 (2017) 41242. doi:10.1038/srep41242.

[6] C.C. Piccinetti, C. Montis, M. Bonini, R. Laurà, M.C. Guerrera, G. Radaelli, et al., Transfer of Silica-Coated Magnetic (Fe_3O_4) Nanoparticles Through Food: A Molecular and Morphological Study in Zebrafish, Zebrafish. 11 (2014) 567–579. doi:10.1089/zeb.2014.1037.

[7] A. Salvatore, C. Montis, D. Berti, P. Baglioni, Multifunctional Magnetoliposomes for Sequential Controlled Release, ACS Nano. 10 (2016) 7749–7760. doi:10.1021/acsnano.6b03194.

[8] D. Maiolo, P. Del Pino, P. Metrangolo, W.J. Parak, F. Baldelli Bombelli, Nanomedicine

delivery: does protein corona route to the target or off road?, Nanomedicine. 10 (2015) 3231–3247. doi:10.2217/nnm.15.163.

[9] F. Bertoli, D. Garry, M.P. Monopoli, A. Salvati, K.A. Dawson, The Intracellular Destiny of the Protein Corona: A Study on its Cellular Internalization and Evolution, ACS Nano. 10 (2016) 10471–10479. doi:10.1021/acsnano.6b06411.

[10] I. Canton, G. Battaglia, Endocytosis at the nanoscale, Chem. Soc. Rev. 41 (2012) 2718. doi:10.1039/c2cs15309b.

[11] K. Bacia, D. Scherfeld, N. Kahya, P. Schwille, Fluorescence correlation spectroscopy relates rafts in model and native membranes, Biophys. J. 87 (2004) 1034–1043. doi:10.1529/biophysj.104.040519.

[12] S. Aimon, J. Manzi, D. Schmidt, J.A. Poveda Larrosa, P. Bassereau, G.E. Toombes, Functional reconstitution of a voltage-gated potassium channel in giant unilamellar vesicles., PLoS One. 6 (2011) e25529.

[13] S. Li, N. Malmstadt, Deformation and poration of lipid bilayer membranes by cationic nanoparticles, Soft Matter. 9 (2013) 4969. doi:10.1039/c3sm27578g.

[14] C. Montis, C. Maiolo, I. Alessandri, P. Bergese, D. Berti, Interaction of nanoparticles with lipid membranes: a multiscale perspective, Nanoscale. 6 (2014) 6452–6457.

[15] S. Smeazzetto, F. Tadini-Buoninsegni, G. Thiel, D. Berti, C. Montis, Phospholamban spontaneously reconstitutes into giant unilamellar vesicles where it generates a cation selective channel, Phys. Chem. Chem. Phys. (2016). doi:10.1039/C5CP05893G.

[16] G. Sharma, D.T. Valenta, Y. Altman, S. Harvey, H. Xie, S. Mitragotri, et al., Polymer particle shape independently influences binding and internalization by macrophages, J. Control. Release. 147 (2010) 408–412. doi:10.1016/j.jconrel.2010.07.116.

[17] M.I. Angelova, S. Soléau, P. Méléard, F. Faucon, P. Bothorel, Preparation of giant vesicles by external AC electric fields. Kinetics and applications, in: C. Helm, M. Lösche, H. Möhwald (Eds.), Trends Colloid Interface Sci. VI SE - 29, Steinkopff, 1992: pp. 127–131. doi:10.1007/BFb0116295.

[18] T. McIntosh, Overview of Membrane Rafts, in: T. McIntosh (Ed.), Lipid Rafts SE - 1, Humana Press, 2007: pp. 1–7. doi:10.1007/978-1-59745-513-8_1.

[19] S. Nappini, T. Al Kayal, D. Berti, B. Nord Èn, P. Baglioni, Magnetically triggered release from giant unilamellar vesicles: Visualization by means of confocal microscopy, J. Phys. Chem. Lett. 2 (2011) 713–718. doi:10.1021/jz2000936.

[20] J. Turkevich, P.C. Stevenson, J. Hillier, A study of the nucleation and growth processes in the synthesis of colloidal gold, Discuss. Faraday Soc. 11 (1951) 55–75. doi:10.1039/DF9511100055.

[21] G. Frens, Controlled Nucleation for the Regulation of the Particle Size in Monodisperse Gold Suspensions, Nat. Phys. Sci. 241 (1973) 20–22. doi:10.1038/physci241020a0.

[22] Y. Liu, M.K. Shipton, J. Ryan, E.D. Kaufman, S. Franzen, D.L. Feldheim, et al., Synthesis, stability, and cellular internalization of gold nanoparticles containing mixed peptide-poly(ethylene glycol) monolayers, Anal. Chem. 79 (2007) 2221–2229. doi:10.1021/ac061578f.

[23] M. Brust, M. Walker, D. Bethell, D.J. Schiffrin, R. Whyman, Synthesis of Thiol-derivatised Gold Nanoparticles in Two-phase Liquid-Liquid System, J. Chem. Soc., Chem. Commun. (1994) 801–802. doi:10.1039/c39940000801.

[24] S. Tatur, M. Maccarini, R. Barker, A. Nelson, G. Fragneto, Effect of functionalized gold nanoparticles on floating lipid bilayers, Langmuir. 29 (2013) 6606–6614. doi:10.1021/la401074y.

[25] C. Montis, S. Sostegni, S. Milani, P. Baglioni, D. Berti, Biocompatible Cationic Lipids for the Formulation of Liposomal DNA Vectors, Soft Matter. 10 (2014) 4287–97. doi:10.1039/c4sm00142g.

[26] X. Chen, F. Tian, X. Zhang, W. Wang, Internalization pathways of nanoparticles and their interaction with a vesicle, Soft Matter. 9 (2013) 7592. doi:10.1039/c3sm50931a.

[27] H. Zhang, Q. Ji, C. Huang, S. Zhang, B. Yuan, K. Yang, et al., Cooperative transmembrane penetration of nanoparticles, Sci. Rep. 5 (2015) 1–10. doi:10.1038/srep10525.

[28] D. Pozzi, V. Colapicchioni, G. Caracciolo, S. Piovesana, A.L. Capriotti, S. Palchetti, et al., Effect of polyethyleneglycol (PEG) chain length on the bio-nano-interactions between PEGylated lipid nanoparticles and biological fluids: from nanostructure to uptake in cancer cells., Nanoscale. 6 (2014) 2782–92. doi:10.1039/c3nr05559k.

[29] Y. Yu, S. Granick, Pearling of lipid vesicles induced by nanoparticles, J. Am. Chem. Soc. 131 (2009) 14158–14159. doi:10.1021/ja905900h.

[30] A.M. Alkilany, P.K. Nagaria, C.R. Hexel, T.J. Shaw, C.J. Murphy, M.D. Wyatt, Cellular uptake and cytotoxicity of gold nanorods: Molecular origin of cytotoxicity and surface effects, Small. 5 (2009) 701–708. doi:10.1002/smll.200801546.

[31] R. Michel, M. Gradzielski, Experimental Aspects of Colloidal Interactions in Mixed systems of liposome and inorganic nanoparticle and their applications, Int. J. Mol. Sci. 13 (2012) 11610–11642. doi:10.3390/ijms130911610.

[32] R. Lipowsky, H.-G. Döbereiner, Vesicles in contact with nanoparticles and colloids, Europhys. Lett. 43 (2007) 219–225. doi:10.1209/epl/i1998-00343-4.

[33] D. Maiolo, L. Paolini, G. Di Noto, A. Zendrini, D. Berti, P. Bergese, et al., Colorimetric nanoplasmonic assay to determine purity and titrate extracellular vesicles, Anal. Chem. 87

(2015) 4168–4176. doi:10.1021/ac504861d.

[34] K.L. Chen, G.D. Bothun, Nanoparticles meet cell membranes: Probing nonspecific interactions using model membranes, Environ. Sci. Technol. 48 (2014) 873–880. doi:10.1021/es403864v.

[35] R. Tadmor, The London – van der Waals interaction energy between objects of various geometries, J. Phys. Condens. Mater. 13 (2001) L195–L202.

[36] T. Kim, C.H. Lee, S.W. Joo, K. Lee, Kinetics of gold nanoparticle aggregation: Experiments and modeling, J. Colloid Interface Sci. 318 (2008) 238–243. doi:10.1016/j.jcis.2007.10.029.

[37] A.H. Bahrami, M. Raatz, J. Agudo-Canalejo, R. Michel, E.M. Curtis, C.K. Hall, et al., Wrapping of nanoparticles by membranes, Adv. Colloid Interface Sci. 208 (2014) 214–224. doi:10.1016/j.cis.2014.02.012.

[38] J. Agudo-Canalejo, R. Lipowsky, Critical particle sizes for the engulfment of nanoparticles by membranes and vesicles with bilayer asymmetry, ACS Nano. 9 (2015) 3704–3720. doi:10.1021/acsnano.5b01285.

[39] A.H. Bahrami, R. Lipowsky, T.R. Weikl, The role of membrane curvature for the wrapping of nanoparticles, Soft Matter. 12 (2015) 581–587. doi:10.1039/C5SM01793A.

[40] W.H. Briscoe, Depletion forces between particles immersed in nanofluids, Curr. Opin. Colloid Interface Sci. 20 (2015) 46–53. doi:10.1016/j.cocis.2014.12.002.

[41] L. Vigderman, B.P. Khanal, E.R. Zubarev, Functional Gold Nanorods: Synthesis, Self-Assembly, and Sensing Applications, Adv. Mater. 24 (2012) 4811–4841. doi:10.1002/adma.201201690.

[42] G. Oliviero, S. Federici, P. Colombi, P. Bergese, On the difference of equilibrium constants of DNA hybridization in bulk solution and at the solid-solution interface, J. Mol. Recognit. 24 (2011) 182–187. doi:10.1002/jmr.1019.

[43] J. van Weerd, M. Karperien, P. Jonkheijm, Supported Lipid Bilayers for the Generation of Dynamic Cell-Material Interfaces, Adv. Healthc. Mater. 4 (2015) 2743–2779. doi:10.1002/adhm.201500398.